arXiv:1611.04605v1 [hep-ph] 14 Nov 2016

Looking for possible new physics in $B \to D^{(*)}\tau\nu_\tau$ in light of recent data

Srimoy Bhattacharya,* Soumitra Nandi,† and Sunando K. Patra‡
Indian Institute of Technology, North Guwahati, Guwahati 781039, Assam, India

We study the decays $B \to D^{(*)}\tau\nu_\tau$ in light of the available data from *BABAR*, Belle and LHCb. We divide our analysis into two parts: in one part we fit the form-factors in these decays directly from the data without adding any additional new physics (NP) contributions and compare our fit results with those available from the decays $B \to D^{(*)}\ell\nu_\ell$. We find that the q^2-distributions of the form-factors associated with the pseudo-vector current, obtained from $B \to D^{(*)}\tau\nu_\tau$ and $B \to D^{(*)}\ell\nu_\ell$ respectively, do not agree with each other, whereas the other form-factors are consistent with each other. In the next part of our analysis, we look for possible new effective operators of dimension 6 amongst new vector, scalar, and tensor-type that can best explain the current data in the decays $B \to D^{(*)}\tau\nu_\tau$. We use the information-theoretic approaches, especially of 'Second-order Akaike Information Criterion' (AIC_c) in the analysis of empirical data . Multi-parameter goodness-of-fit tests are done after selecting the best possible scenarios, for cross-validation. We find that it is the contribution from the operator involving right-handed vector current that passes all the selection criteria defined for the best-fit scenario and can successfully accommodate all the available data set.

I. INTRODUCTION

The semitaunic decays $B \to D^{(*)}\tau\nu_\tau$ have drawn a lot of attention in recent years as sensitive probes of NP [1–6]. The present experimental status is summarized in Fig. 1 [7]. Here, $R(D)$ and $R(D^*)$ are defined as

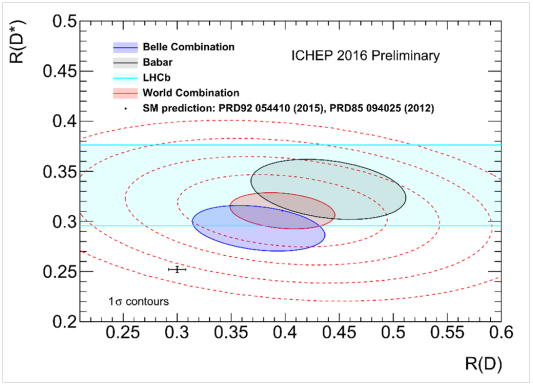

FIG. 1: Current experimental status in the measurements of $R(D)$ and $R(D^*)$.

$$\mathcal{R}(D) = \frac{\mathcal{B}\left(\overline{B} \to D\tau^-\overline{\nu}_\tau\right)}{\mathcal{B}\left(\overline{B} \to Dl^-\overline{\nu}_l\right)} \quad \text{and}$$
$$\mathcal{R}(D^*) = \frac{\mathcal{B}\left(\overline{B} \to D^*\tau^-\overline{\nu}_\tau\right)}{\mathcal{B}\left(\overline{B} \to D^*l^-\overline{\nu}_l\right)}\,. \qquad (1)$$

The Standard Model (SM) predictions for $R(D^{(*)})$ are taken from [4]and [8], respectively. The theory uncertainties in these observables are only a few percent, and independent of the CKM element $|V_{cb}|$. In the figure, the contours show the correlation between the measured values of $R(D)$ and $R(D^*)$ from different experimental collaborations. We note that the contour obtained after averaging the Belle measurements [9–11], which is more than 3σ away from the SM prediction, lies in between the SM expectation and the *BABAR* measurement [12]. LHCb results on $\mathcal{R}(D^*)$ [13] are 2.1σ larger than the value expected in SM. Although the Belle average is slightly smaller than the LHCb and *BABAR* results, it is still considerably larger than the SM prediction.

One can explain this excess by considering the contribution from some NP model of one's choice, *e.g.* [14, 15]. On the other hand, one may write down the most general relevant effective NP operators which may include new scalar, vector and tensor currents other than the SM, and then try to estimate the size of the NP Wilson coefficients from the excess [16] in a model independent analysis.

We observe that with passing time and increasing statistics, the measured value of $R(D^*)$ is becoming closer to that of the SM. However, we have to wait for more precise measurements on $R(D)$. This is important, since the NP sensitivity of $R(D)$ and $R(D^*)$ are not the same [6].

Also, the sensitivity to a particular type of interaction is more apparent in the binned data, compared to that from the integrated observables like $R(D^{(*)})$ [6]. On the other hand, as the measured values of $R(D^{(*)})$ are highly model sensitive due to the model-dependence of the kinetic distribution, one may get different signal yields per bin from fits using different models. Consequently, the measured values obtained from fits assuming only the SM background should not be used to fit the NP parameters. However, it is always safe to use the normalized binned data for NP analysis.

In this article, we systematically divide our analysis into two parts. In the first part of our analysis (section II), we will assume that there is no NP in $B \to D^{(*)}\tau\nu_\tau$, just as in $B \to D^{(*)}\ell\nu_\ell$ ($\ell = e$ or μ), and will fit the form-factors. Different experimental collaborations have already fitted the form-factor parameters [17] from the

* bhattacharyasrimoy@gmail.com
† soumitra.nandi@gmail.com
‡ sunando.patra@gmail.com

data collected for the decays $B \to D^{(*)}\ell\nu_\ell$, *e.g.* [18, 19]. Using the present data on $B \to D^{(*)}\tau\nu_\tau$, we can check whether the fitted form-factors are in good agreement with those obtained from the decay $B \to D^{(*)}\ell\nu_\ell$. Any discrepancy between the two will indicate a possible new effect in $B \to D^{(*)}\tau\nu_\tau$, which is absent in $B \to D^{(*)}\ell\nu_\ell$. It will help us to pinpoint the possible type(s) of new interaction which could be responsible for such deviations.

In the second part of the analysis (section III), we will consider the contributions from different NP interactions in $B \to D^{(*)}\tau\nu_\tau$, but not in $B \to D^{(*)}\ell\nu_\ell$. Our goal will be the search for new interactions most compatible with and best elucidates the present data. Throughout our analysis we will use the q^2-binned data on the decay rate as well the data on $R(D^{(*)})$.

Detailed discussion on our methodology can be found in sections II B, II C, II D and III B.

II. FORM-FACTORS FROM $B \to D^{(*)}\tau\nu_\tau$

A. Formalism

The amplitudes of semileptonic B meson decays can be factorized in the product of the matrix elements of leptonic and hadronic currents. The matrix elements of the hadronic currents are non-perturbative objects called form-factors. For a precise determination of the form-factors, we have to rely either on lattice QCD calculations or on the light cone sum rule approaches (LCSR). The uncertainties in the form-factors is one of the major sources of uncertainties in the predictions of the decay rates.

In the SM, the differential decay rates for the decay $B \to D^{(*)}\ell\nu_\ell$, where $\ell = e,\ \mu$ or τ, are given by [20]

$$\frac{d\Gamma\left(\overline{B} \to D\ell\overline{\nu}_\ell\right)}{dq^2} = \frac{G_F^2\,|V_{cb}|^2}{192\pi^3 m_B^3} q^2 \sqrt{\lambda_D(q^2)} \left(1-\frac{m_\ell^2}{q^2}\right)^2 \left[\left(1+\frac{m_\ell^2}{2q^2}\right) H_{V,0}^{s2} + \frac{3}{2}\frac{m_\ell^2}{q^2} H_{V,t}^{s2}\right], \quad (2)$$

$$\frac{d\Gamma\left(\overline{B} \to D^*\ell\overline{\nu}_\ell\right)}{dq^2} = \frac{G_F^2\,|V_{cb}|^2}{192\pi^3 m_B^3} q^2 \sqrt{\lambda_D^*(q^2)} \left(1-\frac{m_\ell^2}{q^2}\right)^2 \left[\left(1+\frac{m_\ell^2}{2q^2}\right)\left(H_{V,+}^2 + H_{V,-}^2 + H_{V,0}^2\right) + \frac{3}{2}\frac{m_\ell^2}{q^2} H_{V,t}^2\right], \quad (3)$$

where $\lambda_D^{(*)}(q^2) = ((m_B - m_D^{(*)})^2 - q^2)((m_B + m_D^{(*)})^2 - q^2)$. Here, the helicity amplitudes $H_{i,\lambda}^{\lambda_M}$'s are defined through the hadronic matrix elements

$$H_{i,\lambda}^{\lambda_M} = \epsilon_\mu^* \langle M(\lambda_M)|\bar{c}\gamma^\mu(1-\gamma_5)b|\bar{B}\rangle, \quad (4)$$

where λ_M and λ are the helicities of the final state meson M and the virtual intermediate boson in the B meson rest frame respectively. Also note that whereas for D meson $\lambda_M = s$, for D^* meson $\lambda_M = \pm 1,\ 0$ and $\lambda = 0,\ \pm 1$ and t. These helicity amplitudes are related to the form-factors

$$\begin{aligned}
H_{V,0}^s(q^2) &= \sqrt{\frac{\lambda_D(q^2)}{q^2}} F_1(q^2),\\
H_{V,t}^s(q^2) &= \frac{m_B^2 - m_D^2}{\sqrt{q^2}} F_0(q^2),\\
H_{V,\pm}(q^2) &= (m_B + m_{D^*}) A_1(q^2) \mp \frac{\sqrt{\lambda_{D^*}}}{m_B + m_{D^*}} V(q^2),\\
H_{V,0}(q^2) &= \frac{(m_B + m_{D^*})}{2m_{D^*}\sqrt{q^2}} \Big[(m_B^2 - m_{D^*}^2 - q^2) A_1(q^2) + \frac{\lambda_{D^*}}{(m_B + m_{D^*})^2} A_2(q^2)\Big]\\
H_{V,t}(q^2) &= \sqrt{\frac{\lambda_D(q^2)}{q^2}} A_0(q^2)\,. \qquad (5)
\end{aligned}$$

The form-factors are defined as the matrix elements of various currents,

$$\langle D(K)|\bar{c}\gamma_\mu b|\bar{B}(p)\rangle = [(p+k)_\mu - \frac{m_B^2 - m_D^2}{q^2} q_\mu] F_1(q^2) + q_\mu \frac{m_B^2 - m_D^2}{q^2} F_0(q^2)\,, \quad (6)$$

and

$$\begin{aligned}
\langle D^*(k,\varepsilon)|\bar{c}\gamma_\mu b|\bar{B}(p)\rangle &= i\epsilon_{\mu\nu\rho\sigma}\varepsilon^{\nu *} p^\rho k^\sigma \frac{2V(q^2)}{m_B + m_{D^*}}\\
\langle D^*(k,\varepsilon)|\bar{c}\gamma_\mu\gamma_5 b|\bar{B}(p)\rangle &= \varepsilon_\mu^*(m_B + m_{D^*}) A_1(q^2) - (p+k)_\mu (\varepsilon^* q)\frac{A_2(q^2)}{m_B + m_{D^*}}\\
&\quad - q_\mu(\varepsilon^* q)\frac{2m_{D^*}}{q^2}[A_3(q^2) - A_0(q^2]\,, \quad (7)
\end{aligned}$$

where

$$A_3(q^2) = \frac{m_B + m_{D^*}}{2m_{D^*}} A_1(q^2) - \frac{m_B - m_{D^*}}{2m_{D^*}} A_2(q^2)\,. \quad (8)$$

A direct comparison of the matrix elements in eq.(6) with those in heavy quark effective theory (HQET) gives us the relations

$$\begin{aligned}
F_1(q^2) &= \frac{1}{2\sqrt{m_B m_D}}\Big[(m_B + m_D) h_+(w(q^2)) - (m_B - m_D) h_-(w(q^2))\Big]\\
F_0(q^2) &= \frac{1}{2\sqrt{m_B m_D}}\Big[\frac{(m_B + m_D)^2 - q^2}{m_B + m_D} h_+(w(q^2)) - \frac{(m_B - m_D)^2 - q^2}{m_B - m_D} h_-(w(q^2))\Big], \quad (9)
\end{aligned}$$

where $h_\pm(w(q^2))$ are the HQET form-factors, with $w = v_B.v_{D^{(*)}} = \frac{m_B^2 + m_{D^{(*)}}^2 - q^2}{2m_{D^{(*)}} m_B}$. Following the parametrization

given in [17], the HQET form-factors can be expressed as

$$h_+(w) = \frac{1}{2(1+r_D^2-2r_Dw)}\Big[-(1+r_D)^2(w-1)V_1(w) \\ +(1-r_D)^2(w+1)S_1(w)\Big] \\ h_-(w) = \frac{(1-r_D^2)(w+1)}{2(1+r_D^2-2r_Dw)}[S_1(w)-V_1(w)]\,, \quad (10)$$

where $r_D = m_D/m_B$. The hadronic form-factors $V_1(w)$ and $S_1(w)$ coincide with the Isgur-Wise function $\xi(w)$ in the infinite mass limit of the heavy quark m_Q (= m_b or m_c). This function is normalized to unity at zero recoil, i.e at $w = 1$. In the Ref. [17], the w dependence is parameterized as in eq.(11). The idea is to expand $V_1(w)$ around zero recoil point $w = 1$.

$$V_1(w) = V_1(1)\times\left[1-8\rho_D^2 z(w)+(51\rho_D^2-10)z(w)^2 \right. \\ \left. -(252\rho_D^2-84)z(w)^3\right] \quad (11)$$

where $z(w) = (\sqrt{w+1}-\sqrt{2})/(\sqrt{w+1}+\sqrt{2})$. $V_1(1)$ includes corrections at order $\alpha_s(m_Q)$ and Λ_{QCD}/m_Q in HQET. Although $V_1(1)$ cancels in the ratio $R(D)$, it is better to note that lattice QCD can predict the value of $V_1(1) = 1.053 \pm 0.008$ [21]. On the other hand, ρ_D^2 can be fitted directly from the data on $\Gamma(B \to D\ell\nu_\ell)$, where $\ell = e,\ \mu$[1]. As of now, $\rho_D^2 = 1.186 \pm 0.054$, determined by the Heavy Flavor Averaging Group (HFAG) [22].

Following [5], we parameterized the w dependence of $S_1(w)$ as

$$S_1(w) = V_1(w)\times\left\{1+\Delta\left[-0.019+0.041\,(w-1) \right.\right. \\ \left.\left. -0.015\,(w-1)^2\right]\right\}\,. \quad (12)$$

Here, Δ parameterizes the unknown higher order corrections in HQET. In earlier analyses, for the prediction of the $R(D)$, Δ is assumed to have 100% error. The decay rate $\Gamma(B \to D\ell\nu_\ell)$ is not useful to fit the parameters of $S_1(w)$, as it is not sensitive to the decay rates because of the negligible lepton masses. However, in our analysis, we fit Δ from the existing data on $R(D)$ along with the other parameters defined earlier.

As shown in eq. (7), the $B \to D^*\tau\nu$ decays are described by four independent hadronic form-factors: V, A_0, A_1 and A_2, which are related to HQET form-factors by the following relations [4]:

$$V(w) = \frac{R_1(w)}{r_{D^*}}h_{A_1}(w)\,, \\ A_1(w) = \frac{1}{2}r_{D^*}(w+1)h_{A_1}(w)\,, \\ A_2(w) = \frac{R_2(w)}{r_{D^*}}h_{A_1}(w)\,, \\ A_0(w) = \frac{R_0(w)}{r_{D^*}}h_{A_1}(w) \quad (13)$$

where $r_{D^*} = 2\sqrt{m_Bm_{D^*}}/(m_B+m_{D^*})$. The w dependencies of the HQET form-factors are parameterized following the ref. [17],

$$h_{A_1}(w) = h_{A_1}(1)\left[1-8\rho_{D^*}^2 z(w)+(53\rho_{D^*}^2-15)z(w)^2 \right. \\ \left. -(231\rho_{D^*}^2-91)z(w)^3\right]\,, \\ R_1(w) = R_1(1)-0.12(w-1)+0.05(w-1)^2\,, \\ R_2(w) = R_2(1)+0.11(w-1)-0.06(w-1)^2\,, \\ R_0(w) = R_0(1)-0.11(w-1)+0.01(w-1)^2\,. \quad (14)$$

Here, the current lattice prediction is $h_{A_1}(1) = 0.906 \pm 0.013$ [23], the rest of the three parameters like ρ_{D^*}, $R_1(1)$, $R_2(1)$ are fitted directly from the decay rate $\Gamma(B \to D^*\ell\nu_\ell)$ [22],

$$\rho_{D^*}^2 = 1.207 \pm 0.026, \quad C\left(\rho_{D^*}^2,\ R_1(1)\right) = 0.568, \\ R_1(1) = 1.406 \pm 0.033, \quad C\left(\rho_{D^*}^2,\ R_2(1)\right) = -0.809, \\ R_2(1) = 0.853 \pm 0.020,\ C\left(R_1(1),\ R_2(1)\right) = -0.758, \quad (15)$$

where the second column lists the correlations between the parameters. As $B \to D^*\ell\nu$ decays are not sensitive to $R_0(w)$, there is only theoretical estimate available on $R_0(1) = 1.14 \pm 0.07$, based on HQET [4]. However, it can be considered to be a free parameter in our analysis of $B \to D^*\tau\nu$ data.

B. χ^2 analysis

Several parameters parameterizing the form-factors, otherwise not accessible in $\bar{B} \to D^{(*)}\ell^-\bar{\nu}_\ell$ decays, appear in $\bar{B} \to D^{(*)}\tau^-\bar{\nu}_\tau$ decays. By taking the binned data from the q^2-distribution of the decay rates in $\bar{B} \to D^{(*)}\tau^-\bar{\nu}_\tau$ normalized by $d\Gamma(B \to D^{(*)}\ell\nu_\ell)/dq^2$, we fit all the parameters given in section II A. The only exceptions are $V_1(1)$ and $h_{A_1}(1)$ which will cancel in the ratios.

Fig.s 2a and 2b show efficiency-corrected q^2-distributions for $\overline{B} \to D\tau^-\overline{\nu}_\tau$ and $\overline{B} \to D^*\tau^-\overline{\nu}_\tau$ events with $m_{miss}^2 > 1.5$ GeV^2, scaled to results of isospin-constrained fit extracted from the *BABAR* [12] data. The B^0 and B^+ samples are combined and the normalization and background events are subtracted. The uncertainty on the data points includes the statistical uncertainties

[1] From hereon, ℓ will mean light leptons, i.e. e and μ, unless specified otherwise.

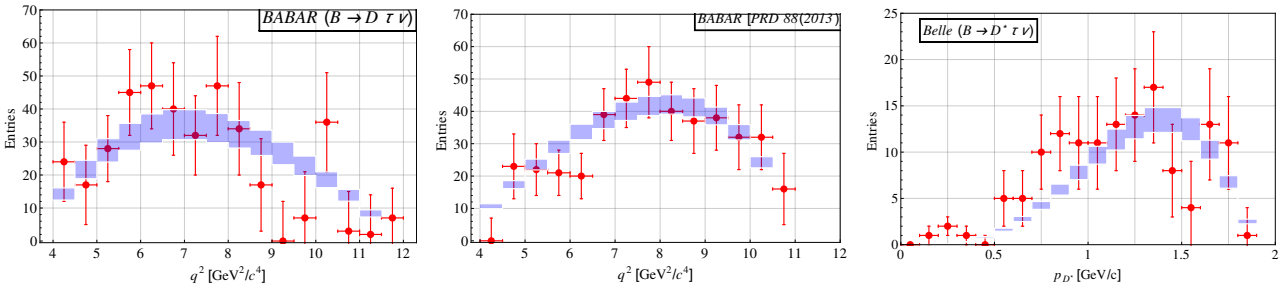

(a) $B \to D\tau\nu$(*BABAR*) (b) $B \to D^*\tau\nu$(*BABAR*) (c) $B \to D^*\tau\nu$(Belle)

FIG. 2: Fig.s 2a and 2b are the measured background subtracted q^2-distributions for $\overline{B} \to D\tau\overline{\nu}_\tau$ and $\overline{B} \to D^*\tau\overline{\nu}_\tau$ events, extracted from the *BABAR* data [12]. Fig. 2c is the background subtracted and normalized momentum distribution of D^* extracted from the Belle data [10]

Experiment	Channel	Input	Value
BABAR [12]	$\overline{B} \to D\tau^-\overline{\nu}_\tau$	N_{sig}	489 ± 63
		N_{norm}	2981 ± 65
		$\epsilon_{sig}/\epsilon_{norm}$	0.372 ± 0.010
	$\overline{B} \to D^*\tau^-\overline{\nu}_\tau$	N^*_{sig}	888 ± 63
		N^*_{norm}	11953 ± 122
		$\epsilon^*_{sig}/\epsilon^*_{norm}$	0.224 ± 0.004
Belle(2016) [10]	$\overline{B} \to D^*\tau^-\overline{\nu}_\tau$	N^*_{sig}	231 ± 23
		N^*_{norm}	2800 ± 57
		$\epsilon^*_{norm}/\epsilon^*_{sig}$	1.289 ± 0.015
LHCb [13]	$\overline{B} \to D^*\tau^-\overline{\nu}_\tau$	$R(D^*)$	$0.336 \pm 0.027 \pm 0.030$
Belle(2015) [9]	$\overline{B} \to D\tau^-\overline{\nu}_\tau$	$R(D)$	$0.375 \pm 0.064 \pm 0.026$
	$\overline{B} \to D^*\tau^-\overline{\nu}_\tau$	$R(D^*)$	$0.293 \pm 0.038 \pm 0.015$
Belle(Latest) [11]	$\overline{B} \to D^*\tau^-\overline{\nu}_\tau$	$R(D^*)$	$0.276 \pm 0.034\ ^{+0.029}_{-0.026}$

TABLE I: Experimental inputs for fits. Only statistical uncertainties are supplied for $N^{(*)}_{norm(sig)}$. Whenever two uncertainties are quoted, they are the statistical and systematic ones respectively.

of data and simulation. Fig. 2c is the background subtracted and normalized momentum distribution of D^* for $\overline{B} \to D^*\tau^-\overline{\nu}_\tau$ events extracted from the Belle [10] data. Here also, the B^0 and B^+ samples are combined and the normalization and background events are subtracted. The light blue histogram represent the SM prediction for the same in each individual bin. We note that both Belle and *BABAR* binned data show deviations from SM predictions.

To fit the parameters of the form-factors, we have performed a test of significance (goodness of fit) by defining a χ^2 statistic, a function of the parameters parameterizing the form-factors, which is defined as

$$\chi^2_{Lat} = \sum_i^{\text{bins}} \frac{\left(R(D^{(*)})^{th}_i - R(D^{(*)})^{exp}_i\right)^2}{\sigma^2_{exp,\ i}}, \qquad (16)$$

where

$$R(D^{(*)})^{th}_{bin} = \frac{\int_{q^2_{\min}}^{q^2_{\max}} \left(d\Gamma\left(\overline{B}\to D^{(*)}\tau^-\overline{\nu}_\tau\right)/dq^2\right)dq^2}{\int_{\text{full } q^2} \left(d\Gamma\left(\overline{B}\to D^{(*)}\ell\overline{\nu}_\ell\right)/dq^2\right)dq^2}, \qquad (17)$$

$$R(D^{(*)})^{exp}_{bin} = \begin{cases} \frac{N^{(*)}_{bin}}{N^{(*)}_{norm}} \times \frac{\epsilon^{(*)}_{norm}}{\epsilon^{(*)}_{sig}} & \textit{BABAR} \\ \frac{1}{2\mathcal{B}(\tau^-\to\ell^-\overline{\nu}_\ell\nu_\tau)} \frac{N^{(*)}_{bin}}{N^{(*)}_{norm}} \times \frac{\epsilon^{(*)}_{norm}}{\epsilon^{(*)}_{sig}} & \text{Belle.} \end{cases} \qquad (18)$$

As input, we consider the central values of number of events, along with their errors, for each q^2 or p_{D^*} bin depending on whether we are analyzing the *BABAR* or the Belle data. The total signal yield $N^{(*)}_{sig}$, along with the errors are given in table I. For simplicity and due to lack of knowledge of q^2-distribution of the efficiencies, we have taken the ratio of efficiencies $\epsilon^{(*)}_{sig}/\epsilon^{(*)}_{norm}$ to be constant over all the q^2 regions and equal to the value shown in table I. In eqs. (17) and (18), $q^2_{max(min)}$ are end points of a particular bin and $\sigma^2_{exp,\ bin}$ is the experimental uncertainty obtained by propagating the uncertainties of individual parts in the l.h.s of eq.(18). For the denominator in eq.(17), we integrate over the whole allowed phase space (from $q^2 = m^2_\ell$ to $q^2 = (m_B - m_{D^{(*)}})^2$).

The Belle results [10] used here is the first measurement of $R(D^*)$ using semileptonic tagging method for the "other B", referred to as B_{tag} and instead of a q^2-distribution, the momentum distribution of D^* and ℓ are given. For our analysis, we note that $p^2_{D^*} = \left(\frac{m^2_B + m^2_{D^*} - q^2}{2m_B}\right)^2 - m^2_{D^*}$, and using this, eq.(17) can be calculated for each bin in the p_{D^*}-distribution by converting the limits of integration appropriately. For $R(D^*)^{exp}_{bin}$, we use eq.(18). We do not use those bins for which central values of $N^{(*)}_{bin} \leq 0$.

The reasons for using eq.(16) as our test statistic are as follows:

1. The systematic correlations between the $q^2(p_{D^*})$-bins are not known to us. In absence of these cor-

relations, the normalization of the χ^2 statistic remains underestimated. We keep that in mind while analyzing the results. As statistical correlations are zero, our covariance matrix is diagonal.

2. To utilize the fact that $V_1(1)$ and $h_{A_1}(1)$ get canceled respectively in $R(D)$ and $R(D^*)$, $R(D^{(*)})_{bin}$ is used instead of $N_{bin}^{(*)}$. So, the χ^2_{Lat} is a function of ρ_D^2 and Δ for $R(D)_{bin}$ and a function of $\rho^2_{D^*}$, $R_1(1)$, $R_2(1)$ and $R_0(1)$ for $R(D^*)_{bin}$.

C. Goodness of Fit

A true model with true parameter values will generate a $\chi^2 = d.o.f$ i.e. $\chi^2_{red} = 1$ as there is no fit involved. But due to noise present in the data, this is not sufficient information to assess convergence or compare different models. The obligatory step to assess the goodness-of-fit of an analysis after optimization is then to inspect the distribution of the residuals. For the true model, with a-priori known measurement errors, the distribution of normalized residuals (in our case, $\frac{R^{th}_{bin} - R^{exp}_{bin}}{\delta R_{bin}}$) is by definition a Gaussian with mean $\mu = 0$ and variance $\sigma^2 = 1$ [24]. This fact is utilized to test the significance of the fit by objectively quantifying a significance test of fitting the distribution of residuals to this Gaussian. For this, instead using only one hypothesis test for the residual-distribution, we made use of 11 such tests distributed with *Mathematica 10.0*, namely, 'Anderson-Darling' (A-D), 'Cramér-von Mises' (C-M), 'Jarque-Bera ALM' (J-B), 'Kolmogorov-Smirnov' (K-S), 'Kuiper' (KU), 'Mardia Combined' (M-C), 'Mardia Kurtosis' (M-K), 'Mardia Skewness' (M-S), 'Pearson χ^2' (CH), 'Shapiro-Wilk' (S-W) and 'Watson U^2' (U2) and compared them. Each of these tests has its qualities and shortcomings; some of them are good for large data samples, some perform poorly with degeneracy in data and so on. In all these tests, the validity of a hypothesis depends on whether the p-value of the goodness of fit test is above or below 5%. Here, p-value is the probability that a random variable having a χ^2-distribution with $d.o.f \geq 1$ assumes a value which is larger than a given value of χ^2 (≥ 0) [25]. Across all the fitted models, the ones with the p-value of the residual-distribution above 5% will be considered to fit the data well; all of the rest can be thrown out. Therefore, if a particular model fitting analysis passes all these tests, we consider that model as the plausible explanation of the data.

D. Fit Results

The fit results for the parameters of the form-factors are listed in table II. We find the distribution of the residuals for all those fits and check whether that distribution is accordant with a normal distribution with mean 0 and variance 1 (with the null hypothesis H_0 that this is true). As shown in fig. 3, the p-values obtained in different tests quantify the probability of H_0 being true. However, for simplicity, in table II, we list only the p-values of the 3 representative tests, namely Kolmogorov-Smirnov, Shapiro-Wilk and Anderson-Darling.

Obs.	Par.s	Value	χ^2_{min}	$d.o.f$	p-val.s for H_0		
					A-D	K-S	S-W
BABAR							
$R(D)_{bin}$	Δ	-0.04 ± 2	9.6	12	0.74	0.78	0.20
	ρ^2_D	1.43 ± 0.18					
$R(D^*)_{bin}$	$\rho^2_{D^*}$	-0.55 ± 0.66	5.4	8	0.46	0.92	0.09
	$R_1(1)$	0.04 ± 2.96					
	$R_2(1)$	3.79 ± 0.20					
	$R_0(1)$	0.02 ± 1.37					
Belle							
$R(D^*)_{bin}$	$\rho^2_{D^*}$	-1.52 ± 1.61	8.7	13	0.50	0.46	0.69
	$R_1(1)$	0.04 ± 2.86					
	$R_2(1)$	3.58 ± 0.53					
	$R_0(1)$	-0.84 ± 0.71					

TABLE II: Fit Results of parameters parameterizing the form-factors in HQET. The last three columns list the results of the hypothesis tests for assessment of goodness-of-fit.

Channel	Correlation	*BABAR*	Belle (2016)
$\overline{B} \to D^* \tau \overline{\nu}_\tau$	$C\left(\rho^2_{D^*},\ R_1(1)\right)$	0.057	0.023
	$C\left(\rho^2_{D^*},\ R_2(1)\right)$	0.907	0.928
	$C\left(\rho^2_{D^*},\ R_0(1)\right)$	-0.004	-0.741
	$C\left(R_1(1),\ R_2(1)\right)$	0.082	0.024
	$C\left(R_1(1),\ R_0(1)\right)$	0.000	-0.008
	$C\left(R_2(1),\ R_0(1)\right)$	0.007	-0.861
$\overline{B} \to D \tau \overline{\nu}_\tau$	$C\left(\Delta,\ \rho^2_D\right)$	0.146	-

TABLE III: Correlations between the fitted form-factor parameters.

After the minimization, we find the uncertainties of and correlations between the parameters around their best fit points. A general approach to find these is to construct the 'Hessian Matrix' H, which is the matrix of second order partial-derivatives of the test-statistic with respect to the parameters; this describes the local curvature of a function of many variables, and find its inverse. This constitutes the 'error matrix', square roots of whose diagonal elements give us the 'standard error' of the parameters and the normalized matrix (w.r.t the errors) makes the 'correlation matrix'. We define such errors and correlations in each case of our analysis, and those are quoted in tables II and III respectively.

In the following we will discuss the outcome of our analysis, and compare our fit results with that determined by HFAG [22] (also given in eq. (15)):

- We fit ρ^2_D only using the *BABAR* data, the obtained value is consistent with that determined by

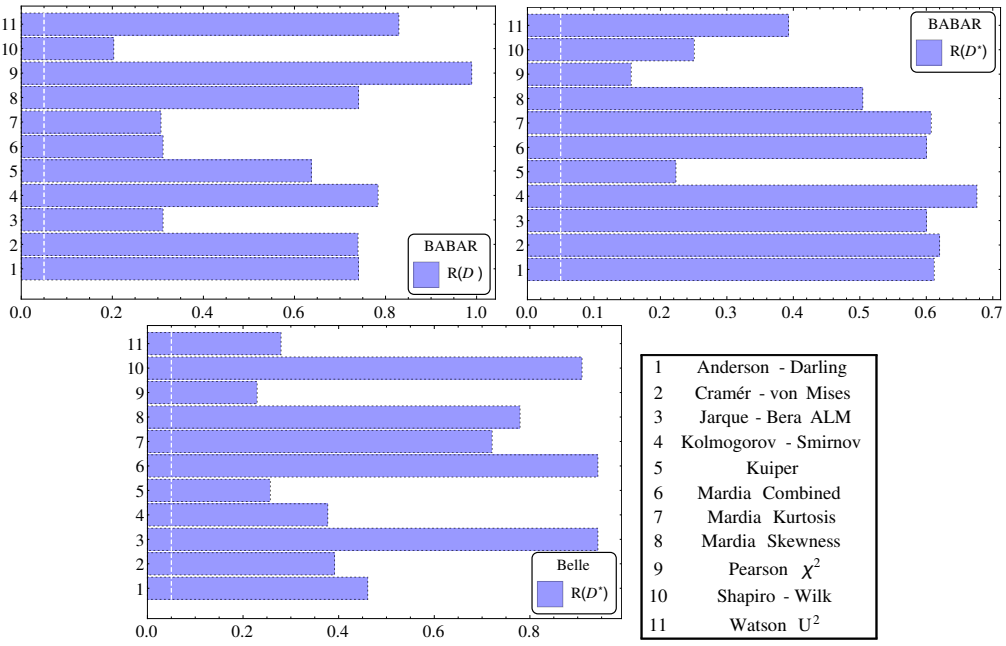

FIG. 3: Hypothesis testing for the model fit of the lattice parameters. Each plot shows the performance of the null-hypothesis H_0 (that the residuals after each fit follow a Gaussian with $\mu = 0$ and $\sigma^2 = 1$). The dotted white vertical line represents the p-value of 5%. The horizontal bars show the performance of H_0 under a specific hypothesis test. Tests are listed according to their assigned numbers.

the HFAG at 1σ. Our fitted value of Δ includes $\Delta = 1 \pm 1$, so far, which is used in the prediction of $R(D)$ by *BABAR* [12].

- The analysis of the *BABAR* bin data on $R(D^*)$ shows that the fitted parameters like $\rho^2_{D^*}$ and $R_1(1)$ are consistent within 2σ, with HFAG. However, $R_2(1)$ shows a large deviation (more than 10σ away). It is important to note that we can extract $R_2(1)$ with relatively small error.

- After analyzing the data by Belle on $R(D^*)$, we obtain large errors on $\rho^2_{D^*}$ and $R_1(1)$, and they are consistent with the fitted value by HFAG at 1σ. Also in this case, $R_2(1)$ fits with a small error, and shows a large deviation from that determined by HFAG.

- Moreover, the analysis of $R(D^*)$ shows that the fit results obtained using *BABAR* and Belle binned data (table II) are consistent with each other, including the best-fit values of $R_0(1)$.

We note that across all the cases listed in table II, $R_2(1)$ can be fitted with a small error and has large deviations from the value obtained from the analysis of $B \to D^*\ell\nu_\ell$ (eq. (15)). All other parameters are extracted with relatively larger errors and are consistent with the fit results obtained by HFAG within 68% or 90% confidence levels (C.L.).

The consequence of these results are reflected in the q^2 dependences of the various form-factors, as shown in fig. 4. In these figures we have compared the q^2-distribution of the form-factors obtained from our fit results with those obtained using the values given in and around eq. (15). As there is some agreement between the ρ^2_D fitted from $B \to D\tau\nu_\tau$ and $B \to D\ell\nu_\ell$, the q^2-distributions of $V_1(q^2)$ and $S_1(q^2)$, shown in figs. 4a and 4b respectively, do not show any considerable deviation. In the analysis of $R(D^*)$, $V(q^2)$ depends on $R_1(1)$ and $\rho^2_{D^*}$, its q^2-distribution has large error and is consistent with those fitted from $B \to D^*\ell\nu_\ell$. $A_1(q^2)$ depends on $\rho^2_{D^*}$ and its q^2-distribution does not show any considerable deviation from that obtained from $B \to D^*\ell\nu_\ell$ fit. As q^2-distributions of both these form-factors obtained from our analysis have large errors, at the moment it is hard to conclude anything and we have to wait for more precise data. On the other hand, among the form-factors associated with $B \to D^*\tau\nu_\tau$, $A_2(q^2)$ depend on $R_2(1)$ and hence it shows large deviation (in all the q^2 regions) from the analysis of $B \to D^*\ell\nu_\ell$ decay. If we assume that the $B \to D^{(*)}\ell\nu_\ell$ decays are free from any kind of NP effects, which may be a natural assumption, then our results allow the possibility of a new contribution beyond the SM in $B \to D^*\tau\nu_\tau$ decay. In particular, it could be a beyond-the-SM (BSM) contribution from a pseudo-vector or a pseudo-tensor [2] current. On a simi-

[2] The pseudo-scalar and pseudo-tensor currents are related to the pseudo-vector currents following the equation of motions, $i\partial_\mu(\bar{c}\gamma^\mu\gamma^5 b) = -(m_b + m_c)\bar{c}\gamma^\mu b$ and $\partial_\mu(\bar{c}\sigma^{\mu\nu}\gamma^5 b) = (m_b -$

lar note, we can comment that the SM contributions in $B \to D\tau\nu_\tau$ can explain the observed data.

III. NEW PHYSICS ANALYSIS

A. Formalism: Theory

We follow a model independent approach in the search of the type of NP interactions that can best explain the present data on $B \to D^{(*)}\tau\nu_\tau$. The most general effective Hamiltonian describing the $b \to c\ell\nu_\ell$ transitions (where $\ell = e$, μ or τ) with all possible four-fermion operators in the lowest dimension is given by [6],

$$\begin{aligned}\mathcal{H}_{eff} = \frac{4G_F}{\sqrt{2}} V_{cb}\Big[&(\delta_{\ell\tau} + C^\ell_{V_1})\mathcal{O}^\ell_{V_1} + C^\ell_{V_2}\mathcal{O}^\ell_{V_2} \\ &+ C^\ell_{S_1}\mathcal{O}^\ell_{S_1} + C^\ell_{S_2}\mathcal{O}^\ell_{S_2} + C^\ell_T\mathcal{O}^\ell_T\Big],\end{aligned} \tag{19}$$

where the operator basis is defined as

$$\begin{aligned}\mathcal{O}^\ell_{V_1} &= (\bar{c}_L\gamma^\mu b_L)(\bar{\tau}_L\gamma_\mu\nu_{\ell L}), \\ \mathcal{O}^\ell_{V_2} &= (\bar{c}_R\gamma^\mu b_R)(\bar{\tau}_L\gamma_\mu\nu_{\ell L}), \\ \mathcal{O}^\ell_{S_1} &= (\bar{c}_L b_R)(\bar{\tau}_R\nu_{\ell L}), \\ \mathcal{O}^\ell_{S_2} &= (\bar{c}_R b_L)(\bar{\tau}_R\nu_{\ell L}), \\ \mathcal{O}^\ell_T &= (\bar{c}_R\sigma^{\mu\nu} b_L)(\bar{\tau}_R\sigma_{\mu\nu}\nu_{\ell L}),\end{aligned} \tag{20}$$

and the corresponding Wilson coefficients are given by C^ℓ_W ($W = V_1, V_2, S_1, S_2, T$). In this basis, neutrinos are assumed to be left handed. The complete expressions for the q^2-distributions of the differential decay rates $d\Gamma/dq^2$ in $B \to D^{(*)}\tau\nu_\tau$ decays, obtained using the effective Hamiltonian in eq.(19), are given by [15]

$$\begin{aligned}\frac{d\Gamma\left(\overline{B} \to D\tau\overline{\nu}_\tau\right)}{dq^2} = \frac{G_F^2\left|V_{cb}\right|^2}{192\pi^3 m_B^3} q^2\sqrt{\lambda_D(q^2)}\left(1-\frac{m_\tau^2}{q^2}\right)^2 \Bigg\{&\left|1+C_{V_1}+C_{V_2}\right|^2\left[\left(1+\frac{m_\tau^2}{2q^2}\right)H_{V,0}^{s2} + \frac{3}{2}\frac{m_\tau^2}{q^2}H_{V,t}^{s2}\right] \\ &+\frac{3}{2}\left|C_{S_1}+C_{S_2}\right|^2 H_S^{s2} + 8\left|C_T\right|^2\left(1+\frac{2m_\tau^2}{q^2}\right)H_T^{s2} + 3\mathcal{R}e\left[\left(1+C_{V_1}+C_{V_2}\right)\left(C_{S_1}^*+C_{S_2}^*\right)\right]\frac{m_\tau}{\sqrt{q^2}}H_S^s H_{V,t}^s \\ &-12\mathcal{R}e\left[\left(1+C_{V_1}+C_{V_2}\right)C_T^*\right]\frac{m_\tau}{\sqrt{q^2}}H_T^s H_{V,0}^s\Bigg\},\end{aligned} \tag{21}$$

and

$$\begin{aligned}\frac{d\Gamma\left(\overline{B} \to D^*\tau\overline{\nu}_\tau\right)}{dq^2} = \frac{G_F^2\left|V_{cb}\right|^2}{192\pi^3 m_B^3} q^2\sqrt{\lambda_D^*(q^2)}\left(1-\frac{m_\tau^2}{q^2}\right)^2 \Bigg\{&\left(\left|1+C_{V_1}\right|^2+\left|C_{V_2}\right|^2\right)\left[\left(1+\frac{m_\tau^2}{2q^2}\right)\left(H_{V,+}^2+H_{V,-}^2+H_{V,0}^2\right)\right. \\ &\left.+\frac{3}{2}\frac{m_\tau^2}{q^2}H_{V,t}^2\right] - 2\mathcal{R}e\left[\left(1+C_{V_1}\right)C_{V_2}^*\right]\left[\left(1+\frac{m_\tau^2}{2q^2}\right)\left(H_{V,0}^2+2H_{V,+}H_{V,-}\right)+\frac{3}{2}\frac{m_\tau^2}{q^2}H_{V,t}^2\right] + \frac{3}{2}\left|C_{S_1}-C_{S_2}\right|^2 H_S^2 \\ &+8\left|C_T\right|^2\left(1+\frac{2m_\tau^2}{q^2}\right)\left(H_{T,+}^2+H_{T,-}^2+H_{T,0}^2\right) + 3\mathcal{R}e\left[\left(1+C_{V_1}-C_{V_2}\right)\left(C_{S_1}^*-C_{S_2}^*\right)\right]\frac{m_\tau}{\sqrt{q^2}}H_S H_{V,t} \\ &-12\mathcal{R}e\left[\left(1+C_{V_1}\right)C_T^*\right]\frac{m_\tau}{\sqrt{q^2}}\left(H_{T,0}H_{V,0}+H_{T,+}H_{V,+}-H_{T,-}H_{V,-}\right) \\ &+12\mathcal{R}e\left[C_{V_2}C_T^*\right]\frac{m_\tau}{\sqrt{q^2}}\left(H_{T,0}H_{V,0}+H_{T,+}H_{V,-}-H_{T,-}H_{V,+}\right)\Bigg\}.\end{aligned} \tag{22}$$

The q^2-distribution of the decay rate of the decays $B \to D^{(*)}\ell\nu_\ell$ are obtained from equations (21) and (22) by setting $C_W = 0$ and $m_\tau = 0$. we define our observables as given in equations (17) and (18).

$m_c)\bar{c}\gamma^\mu b - (i\partial_\mu\bar{c})b + \bar{c}(i\partial_\mu b)$, respectively. Hence, the form-factors associated with the pseudo-scalar and pseudo-tensor are related to $A_0(q^2)$ and/or $A_2(q^2)$. Therefore, a large deviation in $A_2(q^2)$ can also be compensated by adding pseudo-tensor current contributions, proportional to these form-factors, in the decay width.

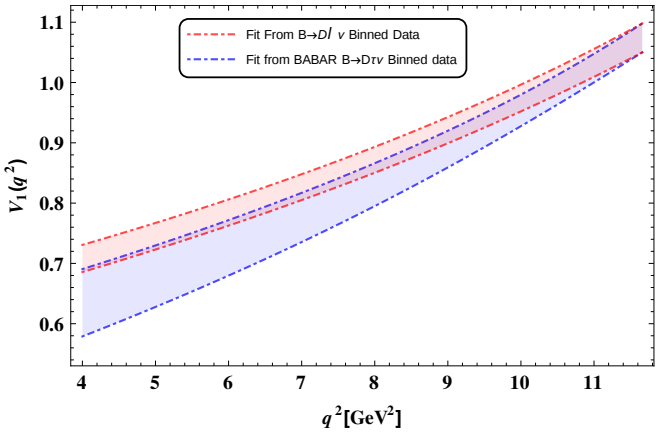

(a) $R(D)_{bin}$

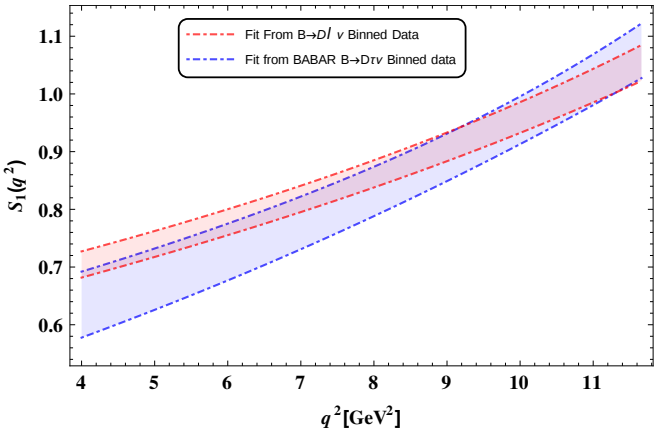

(b) $R(D)_{bin}$

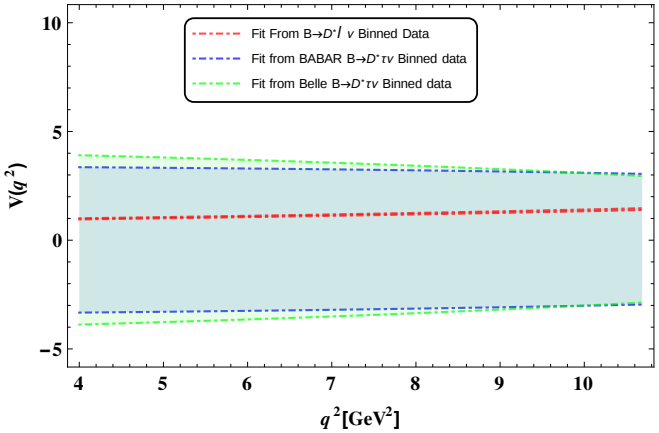

(c) $R(D^*)_{bin}$

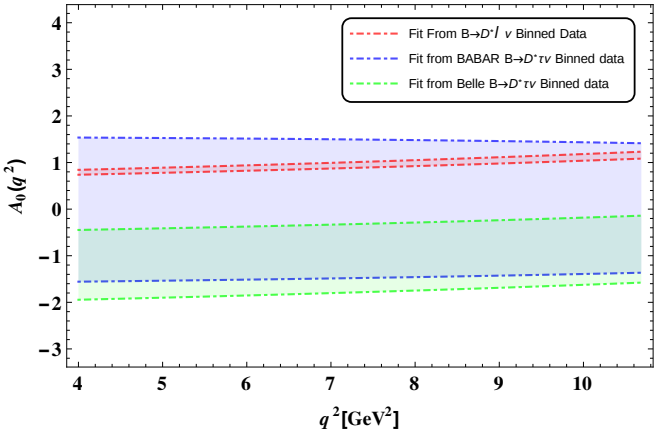

(d) $R(D^*)_{bin}$

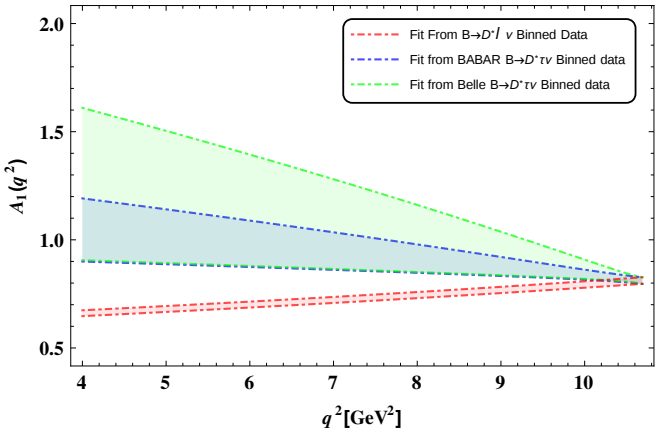

(e) $R(D^*)_{bin}$

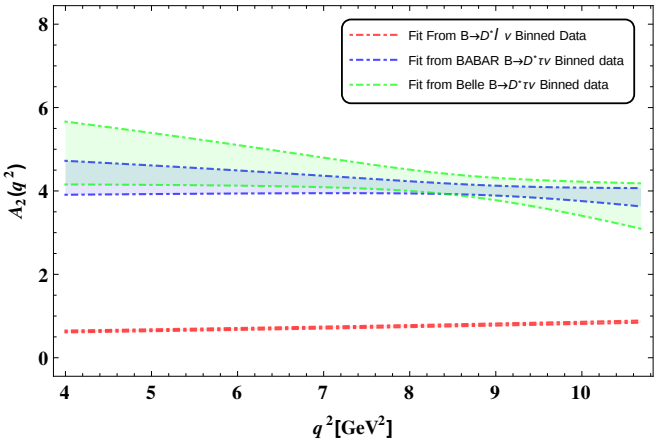

(f) $R(D^*)_{bin}$

FIG. 4: Fig.s 4a and 4b are the q^2 dependence of form-factors for semileptonic $b \to c$ transitions. Red (dotted) and blue (dot-dashed) lines enclose $\pm 1\sigma$ regions for the form-factors with parameters fitted from $\overline{B} \to D\ell\overline{\nu}_\ell$ (world average) and $\overline{B} \to D\tau\overline{\nu}_\tau$ decays (*BABAR*) respectively. The rest of the figures are for form-factors for $\overline{B} \to D^*\ell\overline{\nu}_\ell$ and $\overline{B} \to D^*\tau\overline{\nu}_\tau$ decays. Here green (solid) lines enclose the region for $\overline{B} \to D^*\tau\overline{\nu}_\tau$ decays (Belle).

B. Methodology

We know that the yield in each bin depends on the probability density functions (PDFs) of different (56 in case of *BABAR*) signal and background sources. Considering any NP contribution changes these PDFs and they in turn change the two dimensional $m^2_{miss} - |\mathbf{p}^*_l|$ distributions. This change is reflected in the q^2-distribution as well, because of the following relation: $m^2_{miss} = (q - p_l)^2$. A complete and simultaneous fit to all PDFs can only be done for each specific NP model separately and the dependence of the shape and normalization of the PDFs on the NP parameters should be extracted rigorously using raw experimental data. Without the aid of simulation, we do not attempt to do such an analysis. Instead, we use the background subtracted and normalized binned data for q^2 and p_{D^*}-distributions as depicted in Fig.s 2a, 2b and 2c to perform a phenomenological analysis in a model independent way.

In addition to the binned data from *BABAR* and Belle, we also have the total $R(D^{(*)})$ data from various experiments (see table I). Keeping in mind that the binned data is going to dominate the fit results, we take different combinations of these separate data points and do the whole analysis separately for them.

At the beginning of our analysis, we have defined the most general scenario with contributions from all possible dimension 6 effective operators present simultaneously (with 10 parameters i.e. real and imaginary parts of all C^l_Ws) as the global scenario. We have defined various sub-scenarios as different possible combinations of those operators. Including the global scenario, there are in total 31 such scenarios, which we are going to call "cases" from here onwards.

One of the main motivations of this paper is to do a multi-scenario analysis on the experimentally available binned data, to obtain a data-based selection of a 'best' case and ranking and weighting of the remaining cases in the predefined set of 31. To that goal, we have made use of information-theoretic approaches, especially of AIC_c in the analysis of empirical data. Such procedures lead to more robust inferences in simultaneous comparative analysis of multiple competing scenarios. Traditional statistical inference(e.g. confidence levels, errors on fit parameters, bias etc.) can then be obtained based on the selected best models.[3].

[3] One of the most powerful and most reliable methods for model comparison (also computationally expensive) is 'cross-validation' [24]. The most straightforward (and also most expensive) flavor of cross-validation is leave-one-out cross-validation (LOOCV). It simultaneously tests the predictive power of the model as well minimizes the bias and variance together. In LOOCV, one of the data points is left out and the rest of the sample ("training set") is optimized. Then that result is used to find the predicted residual for the left out data point. This process is repeated for all data points and a mean-squared-error (MSE) is obtained. For model selection, this MSE is minimized. It has been shown that this method is asymptotically equivalent to minimizing AIC [28]

Δ_i^{AIC}	Level of Empirical Support for Model i
$0-2$	Substantial
$4-7$	Considerably Less
>10	Essentially None

TABLE IV: Rough rule-of-thumb values of Δ_i^{AIC} for analysis of nested models.

Input	Value
Δ	1 ± 1 [5]
ρ^2_D	1.186 ± 0.054 [22]
$\rho^2_{D^*}$	1.207 ± 0.026 [22]
$R_1(1)$	1.406 ± 0.033 [22]
$R_2(1)$	0.853 ± 0.020 [22]
$R_0(1)$	1.14 ± 0.07 [4]
$V_1(1)$	1.053 ± 0.008 [21]
$h_{A_1}(1)$	0.906 ± 0.013 [23]
m_{B_0}	$5.27958 \pm 0.00015 \pm 0.00028$ [26]
m_{D_0}	1.86484 ± 0.00005 [27]
m_b	4.18 ± 0.03 [27]
m_c	1.275 ± 0.025 [27]
m_τ	1.77682 ± 0.00012 [27]

TABLE V: Inputs used in the fitting of new Wilson coefficients. All Masses are in GeV. Correlations between a few form-factor parameters are listed in eq. (15).

1. A Short Introduction to AIC_c

The 'concept of parsimony' [29] dictates that a model representing the truth should be obtained with "... the smallest possible number of parameters for adequate representation of the data." In general, bias decreases and variance increases as the dimension of the model increases. Often, the number of parameters in a model is used as a measure of the degree of structure inferred from the data. The fit of any model can be improved by increasing the number of parameters. Parsimonious models achieve a proper trade-off between bias and variance. All model selection methods are based to some extent on the principle of parsimony [30].

In information theory, the Kullback-Leibler (K-L) Information or measure $I(f, g)$ denotes the information lost when g is used to approximate f. Here f is a notation for full reality or truth and g denotes an approximating model in terms of probability distribution. $I(f, g)$ can also be defined between the 'best' approximating model and a competing one. Akaike, in his seminal paper [31] proposed the use of the K-L information as a fundamental basis for model selection. However, K-L distance cannot be computed without full knowledge of both f (full reality) and the parameters (Θ) in each of the candidate models $g_i(x|\Theta)$ (a model g_i with parameter-set Θ explaining data x). Akaike found a rigorous way to estimate K-L

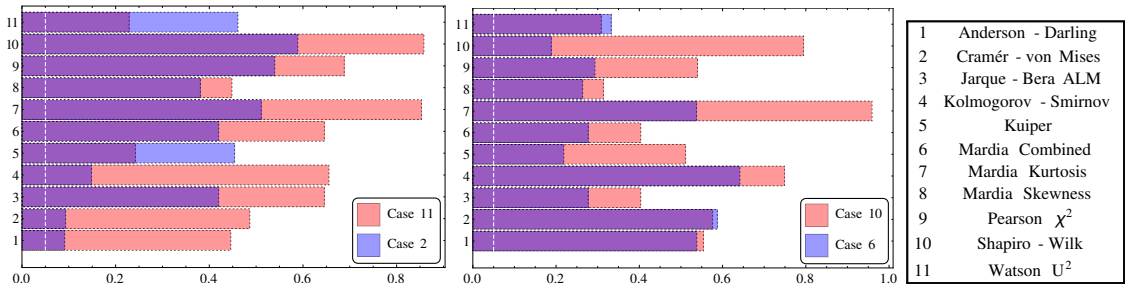

FIG. 5: Hypothesis testing in the selection of best NP scenarios. Each plot shows the performance of the null-hypothesis H_0 (that the residuals after each fit follow a Gaussian with $\mu = 0$ and $\sigma^2 = 1$). The dotted white vertical line represents the p-value of 5%. The horizontal bars show the performance of H_0 under a specific hypothesis test. Tests are listed according to their assigned numbers.

Experiment	Dataset Index.	Observable	Cases	χ^2_{min}	$d.o.f$	Parameters	w_i	p-val.s for H_0		
								A-D	K-S	S-W
BABAR	1	$R(D)_{bin}$	5	7.41	12	C_T	0.26	0.79	0.91	0.38
			1	7.79	12	C_{V_1}	0.22	0.83	0.90	0.29
			2	7.79	12	C_{V_2}	0.22	0.83	0.90	0.29
			3	9.17	12	C_{S_1}	0.11	0.79	0.83	0.18
			4	9.17	12	C_{S_2}	0.11	0.79	0.83	0.18
	2	$R(D^*)_{bin}$	1	6.3	10	C_{V_1}	0.56	0.49	0.36	0.11
			2	7.18	10	C_{V_2}	0.36	0.51	0.25	0.12
	3	Combined	8	13.01	22	C_{V_2}, C_{S_2}	0.32	0.45	0.66	0.86
			2	19.12	24	C_{V_2}	0.22	0.09	0.15	0.59
			7	14.23	22	C_{V_2}, C_{S_1}	0.17	0.55	0.75	0.79
			6	14.61	22	C_{V_1}, C_{V_2}	0.14	0.54	0.64	0.19
Belle(2016)	4	$R(D^*)_{bin}$	2	9.07	15	C_{V_2}	0.47	0.48	0.52	0.95
			1	9.43	15	C_{V_1}	0.39	0.50	0.52	1.00
BABAR+ Belle(2016)	5	Combined	8	22.59	39	C_{V_2}, C_{S_2}	0.31	0.15	0.26	0.95
			2	28.33	41	C_{V_2}	0.19	0.34	0.27	0.94
			7	23.69	39	C_{V_2}, C_{S_1}	0.18	0.18	0.38	0.89
			6	24.16	39	C_{V_1}, C_{V_2}	0.14	0.20	0.32	0.69
BABAR+ Belle(2015)+ LHCb+ Belle(Latest)	6	Combined	2	48.54	28	C_{V_2}	0.52	0.12	0.15	0.02
			8	45.71	26	C_{V_2}, C_{S_2}	0.16	0.39	0.01	0.4
			7	46.87	26	C_{V_2}, C_{S_1}	0.09	0.39	0.70	0.02
			6	47.24	26	C_{V_1}, C_{V_2}	0.08	0.52	0.69	0.04
Belle(2016)+ LHCb+ Belle(Latest)	7	Combined	2	24.18	17	C_{V_2}	0.47	0.72	0.62	0.25
			1	25.64	17	C_{V_1}	0.23	0.71	0.73	0.35

TABLE VI: Results obtained on the best selected scearios. The cases listed in fourth column for each dataset pass through the selection criteria $0 \leq \Delta_i^{AIC} \leq 4$, where $\Delta_1^{AIC} = 0$ in each dataset. Note that the case-index values represent a specific set of parameters and each parameter listed here is considered to be complex, so the number of parameters is actually double. w_i in the eighth column is defined in eq.(26). The last three columns list the results of the hypothesis tests for assessment of goodness-of-fit.

information, based on the empirical log-likelihood function at its maximum point.

'Akaike's information criterion'(AIC) with respect to our analysis can be defined as,

$$\text{AIC} = \chi^2_{min} + 2K \tag{23}$$

where K is the number of estimable parameters. In application, one computes AIC for each of the candidate models and selects the model with the smallest value of AIC. It is this model that is estimated to be "closest" to the unknown reality that generated the data, from among the candidate models considered.

While Akaike derived an estimator of K-L information, AIC may perform poorly if there are too many parameters in relation to the size of the sample. Sugiura[32]

derived a second-order variant of AIC,

$$\mathrm{AIC}_c = \chi^2_{min} + 2K + \frac{2K(K+1)}{n-K-1} \tag{24}$$

where n is the sample size. As a rule of thumb, Use of AIC_c is preferred in literature when $n/K < 40$. There are various other such information criteria defined later on, e.g. QAIC, QAIC_c, TIC etc. In this analysis, we consistently use AIC_c.

Whereas AIC_c are all on a relative (or interval) scale and are strongly dependent on sample size, simple differences of AIC_c values ($\Delta_i^{AIC} = \mathrm{AIC}_c^i - \mathrm{AIC}_c^{min}$) allow estimates of the relative expected K-L differences between f and $g_i(x|\Theta)$. This allows a quick comparison and ranking of candidate models. The model estimated to be best has $\Delta_i^{AIC} \equiv \Delta_{min}^{AIC} = 0$. The larger Δ_i^{AIC} is, the less plausible it is that the fitted model $g_i(x|\Theta)$ is the K-L best model, given the data x. Table IV lists rough rule-of-thumb values of Δ_i^{AIC} for analysis of nested models.

While the Δ_i^{AIC} are useful in ranking the models, it is possible to quantify the plausibility of each model as being the actual K-L best model. This can be done by extending the concept of the likelihood of the parameters given both the data and model, i.e. $\mathcal{L}(\Theta|x, g_i)$, to the concept of the likelihood of the model given the data, hence $\mathcal{L}(g_i|x)$;

$$\mathcal{L}(g_i|x) \propto e^{(-\Delta_i^{AIC}/2)}\,. \tag{25}$$

Such likelihoods represent the relative strength of evidence for each model [33].

To better interpret the relative likelihood of a model, given the data and the set of R models, we normalize the $\mathcal{L}(g_i|x)$ to be a set of positive Akaike weights, w_i , adding up to 1:

$$w_i = \frac{e^{(-\Delta_i^{AIC}/2)}}{\sum_{r=1}^{R} e^{(-\Delta_r^{AIC}/2)}} \tag{26}$$

A given w_i is considered as the weight of evidence in favor of model i being the actual K-L best model for the situation at hand, given that one of the R models must be the K-L best model of that set. The w_i depend on the entire set; therefore, if a model is added or dropped during a post hoc analysis, the w_i must be recomputed for all the models in the newly defined set.

2. Numerical Multi-parameter Optimization

To compare the latest *BABAR* and Belle binned data with a specific model, we devise a χ^2 defined as:

$$\chi^2_{NP} = \sum_{i,j=1}^{n_b} \left(R_i^{exp} - R_i^{th}\right) \left(V^{exp} + V^{th}\right)^{-1}_{ij} \left(R_j^{exp} - R_j^{th}\right)\,, \tag{27}$$

where R_{bin}^{th} and R_{bin}^{exp} are defined in eq.s (17) and (18). i and j vary over the number of bins (n_b) taken into account in the analysis. For the calculation of R_{bin}^{th}, central values of HQET hadronic form-factors and the quark masses are used (listed in table V). The standard bin-width for the *BABAR* analysis is $0.5(\mathrm{GeV}^2/c^4)$ and due to this the last bin exceeds the allowed phase space($q^2_{max} = (m_B - m_{D^{(*)}})^2$) in both channels. Instead of changing the bin width for those last bins, we drop these bins from our analysis. We follow this same philosophy for Belle bins too. V_{ij}^{th} and V_{ij}^{exp} are the theoretical and experimental covariance matrices respectively. For the analysis of any specific NP model, the uncertainties of the HQET hadronic form-factors and the quark masses(table V) are taken into account in the calculation of V_{ij}^{th}.

To calculate the errors δR_{bin}^{exp}, we use eq.(18) according to the case and propagate the errors listed in table I. In defining V_{ij}^{exp}, we make following assumptions

1. We assume correlations to be negligible, i.e. V^{exp} is diagonal.

DataSet Ind.	Cases	Param.s	B.F. Val	± Err.
1	5	$Re(C_T)$	0.27	0.10
		$Im(C_T)$	0.	1.06
	3	$Re(C_{S_1})$	0.09	0.06
		$Im(C_{S_1})$	0.	0.30
	4	$Re(C_{S_2})$	0.09	0.06
		$Im(C_{S_2})$	0.	0.30
2	2	$Re(C_{V_2})$	0.27	0.03
		$Im(C_{V_2})$	0.	0.40
3	8	$Re(C_{V_2})$	0.34	0.12
		$Im(C_{V_2})$	−0.33	0.20
		$Re(C_{S_2})$	−0.52	0.43
		$Im(C_{S_2})$	−0.16	0.21
	2	$Re(C_{V_2})$	0.23	0.02
		$Im(C_{V_2})$	0.	0.09
	7	$Re(C_{V_2})$	0.29	0.03
		$Im(C_{V_2})$	0.	0.54
		$Re(C_{S_1})$	−0.23	0.09
		$Im(C_{S_1})$	0.	0.48
4	2	$Re(C_{V_2})$	0.58	0.69
		$Im(C_{V_2})$	−0.59	0.37
5	8	$Re(C_{V_2})$	0.34	0.12
		$Im(C_{V_2})$	−0.35	0.21
		$Re(C_{S_2})$	−0.51	0.46
		$Im(C_{S_2})$	−0.14	0.22
	2	$Re(C_{V_2})$	0.23	0.02
		$Im(C_{V_2})$	0.	0.09
	7	$Re(C_{V_2})$	0.28	0.03
		$Im(C_{V_2})$	0.	0.70
		$Re(C_{S_1})$	−0.22	0.08
		$Im(C_{S_1})$	0.	0.55
7	2	$Re(C_{V_2})$	1.16	0.68
		$Im(C_{V_2})$	0.75	0.24

TABLE VII: Best-fit values and Gaussian errors of all parameters for the selected 'best' cases in the NP analysis, listed in table VI. Some cases are omitted due to the reason explained in section II C and corresponding plots are tabulated in fig. 6.

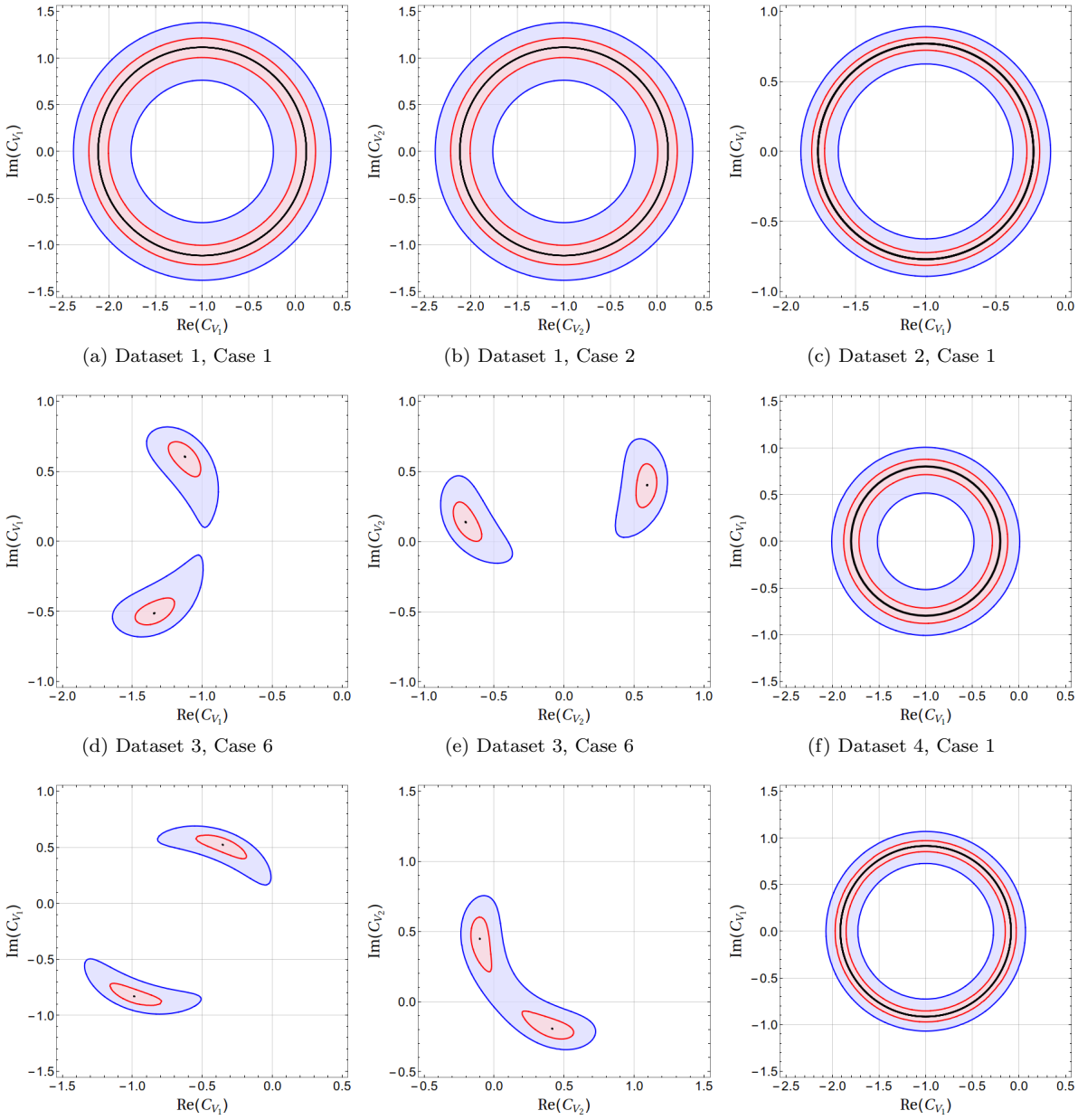

(a) Dataset 1, Case 1 (b) Dataset 1, Case 2 (c) Dataset 2, Case 1

(d) Dataset 3, Case 6 (e) Dataset 3, Case 6 (f) Dataset 4, Case 1

(g) Dataset 5, Case 6 (h) Dataset 5, Case 6 (i) Dataset 7, Case 1

FIG. 6: The 'cases' for different datasets listed in table VI, which pass the goodness-of-fit hypothesis tests but could not be listed in table VII as for these cases, the minimum, instead of being an isolated point, is actually a contour in the parameter-space. Though this is true for all plots listed here, some cases have four parameters and we are only able to show the two-parameter cross-sections of these.(e.g. plots 6d and 6e are actually cross-sections of a single four-dimensional plot. Same is true for 6g and 6h).

2. Statistical and systematic errors are added in quadrature.

So, $V_{ij}^{exp} = \delta_{ij}\ \delta R_i^{exp}\ \delta R_j^{exp}$, where δ_{ij} is the Kronecker delta.

We define the χ^2 statistic for each of the 31 cases, a function of the NP Wilson coefficients. The definition and usage of the observables closely follow the fitting process in section II B. Here, we take the existing world-averages of the parameters of the form-factors [22]. If we include all the NP interactions, we have total 10 unknown NP parameters and 26 observables for *BABAR* (14 bins for $B \to D\tau\nu$ and 12 bins for $B \to D^*\tau\nu$) and 17 observables for Belle. We then minimize the χ^2 for different cases and different set of observables. To optimize the minimization method, we have varied the process for all available global optimization methods (namely, 'Nelder-Mead', 'Differ-

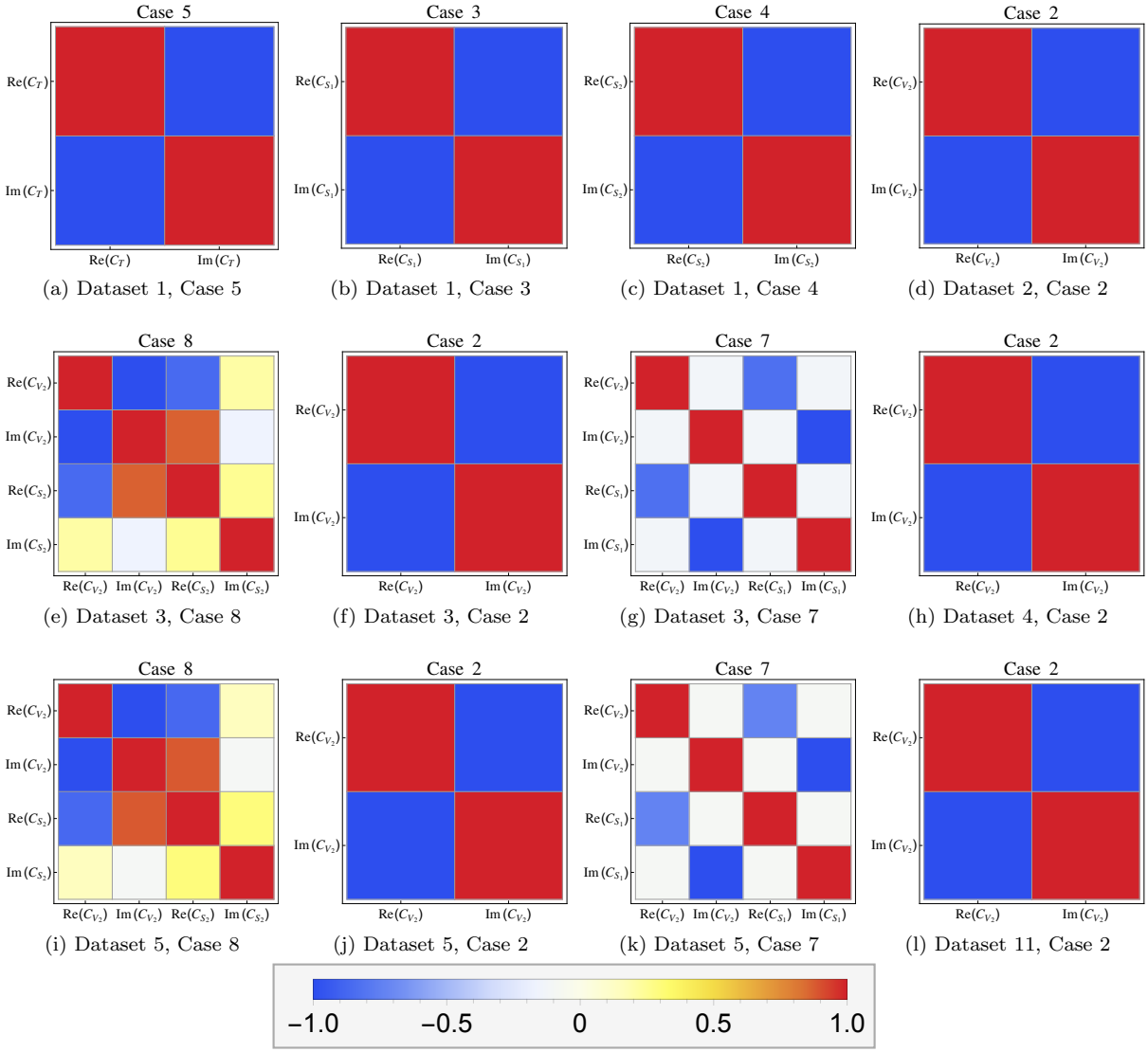

(a) Dataset 1, Case 5 (b) Dataset 1, Case 3 (c) Dataset 1, Case 4 (d) Dataset 2, Case 2

(e) Dataset 3, Case 8 (f) Dataset 3, Case 2 (g) Dataset 3, Case 7 (h) Dataset 4, Case 2

(i) Dataset 5, Case 8 (j) Dataset 5, Case 2 (k) Dataset 5, Case 7 (l) Dataset 11, Case 2

FIG. 7: Array-plots showcasing the correlations between the fitted parameters of separate 'cases' for different datasets listed in table VII. The color-coding is explained in the horizontal legend. As can be seen, for the cases with only two independent parameters, the parameters are strongly (negatively) correlated, compared to other cases, as expected.

ential Evolution', 'Simulated Anealing' and 'Random Search'). These processes have also been looped over significant options (e.g. 'Penalty Function', 'Random Seed', 'Tolerance' etc. for the method Nelder-Mead).

We have found out that in addition to the generic and popular 'Differential Evolution', a set of other optimization methods perform well in fits of this project. As an example, 'Nelder-Mead' (otherwise known as the 'Simplex Method') with 'Shrink-ratio' and 'Contract-ratio' = 0.95 and 'Reflect-ratio'= 2 or 'Random-Search' with 'Search-points' = 700 gives us better result than 'Differential Evolution' in numerous cases. To glean any information of goodness-of-fit from χ^2_{min}, we need to know the degrees of freedom ($d.o.f = N_{Obs} - N_{Params}$). A reduced statistic $\chi^2_{red} = \chi^2_{min}/d.o.f$ can thus be defined.

In many cases in our optimization problem, the minimum is not an isolated single point, rather a contour in the parametric dimensions. For these cases, Hessian in not positive definite and the errors thus obtained are meaningless. In those cases, the 1σ uncertainties have to found from the contours in the parameter space and we have done that for all cases with $2-3$ parameters. As contours are impossible to draw when number of parameters > 3, we have devised a numerical method to obtain the range of a parameter. In this method, we sequentially minimize or maximize each parameter by scanning along the enclosing 1σ χ^2_{NP} hyper-contour-surface (the method can be extended to any number of $n\sigma$ contours). These

values give us the range of each parameter while taking their correlation into account all along. These errors, for obvious reasons, are asymmetric. We have also systematically found these uncertainties for all cases. We will in general quote them in our results.

In our present analysis, after optimizing the χ^2_{NP} for all 31 cases, we make use of Δ_i^{AIC} and w_i to find the 'best' set of cases, which are more favorable compared to others, and do further analysis on them. After selecting a class of models describing the data with optimum bias and variance with AIC_c, we check the significance of them to find most suited model to describe the data.

C. Results

The best models, which are obtained after minimizing the χ^2_{NP} and using w_i (eq. (26)), are listed in table VI. Then using the formalism defined in section II C), we find the distribution of the residuals for all those fits and we check whether that distribution is accordant with a normal distribution with mean 0 and variance 1. In fig. 5, we show a representative comparison chart of p-values for all these tests for dataset-index (3) i.e. the combined binned *BABAR* data, color-coded for the 'best' scenarios found using Akaike-weights. The p-value obtained in any test quantifies the probability of H_0 being true. In table VI, the last three columns list the p-values for three such representative tests: 'Anderson-Darling'(A-D), 'Kolmogorov-Smirnov'(K-S) and 'Shapiro-Wilk'(S-W).

Only those NP scenarios, which passed all the hypothesis tests mentioned in section II C, are listed in table VII with the best-fit values and 1σ uncertainties of their parameters. Other than that, some cases are omitted, where the minimum, instead of being an isolated point, is actually a contour in the parameter-space. For such cases, we have plotted the best-fit contours in the parameter-space. These are shown in fig. 6. After the minimization and selecting the probable NP cases (scenarios) with the help of 'AIC_c', we find the uncertainties of and correlations between the parameters appearing in those cases around the obtained best fit values. The method is similar to that described in section II D.

In fig. 6, we have prepared our plots in terms of the goodness-of-fit contours for joint estimation of multiple NP parameters at a time. 1σ and 4σ contours that are equivalent to p-values of 0.3173 and 0.0001, correspond to confidence levels of 68.27% and 99.99%, respectively. For our purpose, each confidence interval corresponds to a particular value of $X = \Delta\chi^2$ (i.e. $\chi^2 - \chi^2_{min}$) for a particular model with $d.o.f = N_{params}$, where the SM is considered to be the model with no free parameters. For cases up-to 3 parameters, errors on parameters can be estimated from the edges of the 2 or 3 dimensional contours as they properly reflect the correlation between the involved parameters.

From Tables VI and VII, we note that all types of new interactions that we have considered in our analysis can individually explain the data on $R(D)_{bin}$ published by *BABAR*. However, when it comes to the q^2 distribution of decay rate of $B \to D^*\tau\nu_\tau$, both *BABAR* and Belle data independently and together allow a contribution from a new right-handed charged current $(V + A)$ effective operator (case 2) as a plausible explanation. Also, across all the scenarios, which qualify our predefined test criteria, a common NP explanation is case 2, i.e the presence of a new $(V + A)$ type interaction. Here, we can not distinguish whether the new contribution is a vector or a pseudo-vector or both. However, if we combine the information obtained from the parametric fit of the form factors, it won't be wrong to conclude that the most favorable solution of the present data on the decay $B \to D^*\tau\nu_\tau$ could be obtained from the presence of a pseudo-vector current.

IV. SUMMARY

We look for possible new physics effects in the decays $B \to D^{(*)}\tau\nu_\tau$ in the light of the recently available data from Belle, *BABAR* and LHCb. At first, the form-factors, relevant in these decays, are fitted assuming the absence of any contribution coming from operators other than the SM. The fitted results are then compared with those obtained by HFAG from a fitting to the available data on $B \to D^{(*)}\ell\nu_\ell$. We note that the fit results of the parameter $R_2(1)$ largely disagree with each other, while the rest are more or less consistent with each other within errors. The effects are prominent in all the regions of the q^2 distribution of the form-factor $A_2(q^2)$, which is associated with a pseudo-vector current. Therefore, assuming the decays $B \to D^{(*)}\ell\nu_\ell$ are free from any new physics effects, such a difference in the q^2 distribution of A_2 (obtained from $B \to D^*\tau\nu_\tau$ and $B \to D^*\ell\nu_\ell$) can be compensated by adding a contribution from new pseudo vector and/or pseudo tensor currents.

In the next part of our analysis, we consider the new physics contributions in the decays $B \to D^{(*)}\tau\nu_\tau$ which come from new vector, scalar or tensor type operators. In this case, we take the relevant form-factors as obtained using the fit results by HFAG. We define different possible NP scenarios which are obtained after combining contributions from the new operators in many different ways. Our goal is to select the best possible NP scenarios (new interactions) that can accommodate all the available data. In doing so, we use the AIC_c in the analysis of the empirical data. Such procedures lead to more robust inferences in simultaneous comparative analysis of multiple competing scenarios. In order to check whether all the NP scenarios that are coming out of AIC_c test can fit the data well or not, we have done multiple different goodness-of-fit tests for each selected model. Our analysis of $B \to D^*\tau\nu_\tau$ shows that it is the contribution from a right-handed charged vector current effective operator, that, as well as accommodating all the available

data, passes all the selection criteria for being the best possible NP scenario.

Here, we would like to point out that we have made use of the available data on the q^2 (bins) distributions of the decays $B \to D^{(*)}\tau\nu_\tau$, which have large errors. This, in turn, gives our fitted results large errors. Once the more precise data on the q^2 bins are made available, one may and should repeat the analysis to check sustainability of the above conclusions.

ACKNOWLEDGEMENTS

We thank Gabriele Simi (Univ. of Padova) and Devdatta Majumder (Univ. of Kansas) for really helpful discussions on binned data and residual-distributions.

REFERENCES

[1] W. S. Hou, Phys. Rev. D **48**, 2342 (1993). doi:10.1103/PhysRevD.48.2342

[2] C. H. Chen and C. Q. Geng, JHEP **0610**, 053 (2006) doi:10.1088/1126-6708/2006/10/053 [hep-ph/0608166].

[3] U. Nierste, S. Trine and S. Westhoff, Phys. Rev. D **78**, 015006 (2008) doi:10.1103/PhysRevD.78.015006 [arXiv:0801.4938 [hep-ph]].

[4] S. Fajfer, J. F. Kamenik and I. Nisandzic, Phys. Rev. D **85**, 094025 (2012) doi:10.1103/PhysRevD.85.094025 [arXiv:1203.2654 [hep-ph]].

[5] M. Tanaka and R. Watanabe, Phys. Rev. D **82**, 034027 (2010) doi:10.1103/PhysRevD.82.034027 [arXiv:1005.4306 [hep-ph]].

[6] S. Bhattacharya, S. Nandi and S. K. Patra, Phys. Rev. D **93**, no. 3, 034011 (2016) doi:10.1103/PhysRevD.93.034011 [arXiv:1509.07259 [hep-ph]].

[7] Y. Sato [Nagoya Univ.], "Tree-level New Physics searches in semileptonic B decays at Belle" Talk presented at ICHEP 2016.

[8] H. Na *et al.* [HPQCD Collaboration], Phys. Rev. D **92**, no. 5, 054510 (2015) doi:10.1103/PhysRevD.92.054510 [arXiv:1505.03925 [hep-lat]].

[9] M. Huschle *et al.* [Belle Collaboration], Phys. Rev. D **92**, no. 7, 072014 (2015) doi:10.1103/PhysRevD.92.072014 [arXiv:1507.03233 [hep-ex]].

[10] A. Abdesselam *et al.* [Belle Collaboration], arXiv:1603.06711 [hep-ex].

[11] A. Abdesselam *et al.*, arXiv:1608.06391 [hep-ex].

[12] J. P. Lees *et al.* [BaBar Collaboration], Phys. Rev. D **88**, no. 7, 072012 (2013) doi:10.1103/PhysRevD.88.072012 [arXiv:1303.0571 [hep-ex]].

[13] R. Aaij *et al.* [LHCb Collaboration], Phys. Rev. Lett. **115**, no. 11, 111803 (2015) Addendum: [Phys. Rev. Lett. **115**, no. 15, 159901 (2015)] doi:10.1103/PhysRevLett.115.159901, 10.1103/PhysRevLett.115.111803 [arXiv:1506.08614 [hep-ex]].

[14] Y. Sakaki and H. Tanaka, Phys. Rev. D **87**, no. 5, 054002 (2013) doi:10.1103/PhysRevD.87.054002 [arXiv:1205.4908 [hep-ph]]; S. Fajfer, J. F. Kamenik, I. Nisandzic and J. Zupan, Phys. Rev. Lett. **109**, 161801 (2012) doi:10.1103/PhysRevLett.109.161801 [arXiv:1206.1872 [hep-ph]]; A. Datta, M. Duraisamy and D. Ghosh, Phys. Rev. D **86**, 034027 (2012) doi:10.1103/PhysRevD.86.034027 [arXiv:1206.3760 [hep-ph]]; J. A. Bailey *et al.*, Phys. Rev. Lett. **109**, 071802 (2012) doi:10.1103/PhysRevLett.109.071802 [arXiv:1206.4992 [hep-ph]]; D. Beirevi, N. Konik and A. Tayduganov, Phys. Lett. B **716**, 208 (2012) doi:10.1016/j.physletb.2012.08.016 [arXiv:1206.4977 [hep-ph]]; M. Tanaka and R. Watanabe, Phys. Rev. D **87**, no. 3, 034028 (2013) doi:10.1103/PhysRevD.87.034028 [arXiv:1212.1878 [hep-ph]]; M. Freytsis, Z. Ligeti and J. T. Ruderman, Phys. Rev. D **92**, no. 5, 054018 (2015) doi:10.1103/PhysRevD.92.054018 [arXiv:1506.08896 [hep-ph]]; A. Celis, M. Jung, X. Q. Li and A. Pich, JHEP **1301**, 054 (2013) doi:10.1007/JHEP01(2013)054 [arXiv:1210.8443 [hep-ph]]; P. Ko, Y. Omura and C. Yu, JHEP **1303**, 151 (2013) doi:10.1007/JHEP03(2013)151 [arXiv:1212.4607 [hep-ph]]; A. Crivellin, C. Greub and A. Kokulu, Phys. Rev. D **86**, 054014 (2012) doi:10.1103/PhysRevD.86.054014 [arXiv:1206.2634 [hep-ph]]; N. G. Deshpande and A. Menon, JHEP **1301**, 025 (2013) doi:10.1007/JHEP01(2013)025 [arXiv:1208.4134 [hep-ph]]; A. Greljo, G. Isidori and D. Marzocca, JHEP **1507**, 142 (2015) doi:10.1007/JHEP07(2015)142 [arXiv:1506.01705 [hep-ph]]; I. Dorner, S. Fajfer, N. Konik and I. Niandi, JHEP **1311**, 084 (2013) doi:10.1007/JHEP11(2013)084 [arXiv:1306.6493 [hep-ph]]; F. F. Deppisch, T. E. Gonzalo, S. Patra, N. Sahu and U. Sarkar, Phys. Rev. D **90**, no. 5, 053014 (2014) doi:10.1103/PhysRevD.90.053014 [arXiv:1407.5384 [hep-ph]]; S. Fajfer and N. Konik, Phys. Lett. B **755**, 270 (2016) doi:10.1016/j.physletb.2016.02.018 [arXiv:1511.06024 [hep-ph]]; D. Becirevic, S. Fajfer, I. Nisandzic and A. Tayduganov, arXiv:1602.03030 [hep-ph]; J. Zhu, H. M. Gan, R. M. Wang, Y. Y. Fan, Q. Chang and Y. G. Xu, Phys. Rev. D **93**, no. 9, 094023 (2016) doi:10.1103/PhysRevD.93.094023 [arXiv:1602.06491 [hep-ph]]; B. Dumont, K. Nishiwaki and R. Watanabe, Phys. Rev. D **94**, no. 3, 034001 (2016) doi:10.1103/PhysRevD.94.034001 [arXiv:1603.05248 [hep-ph]]; X. Q. Li, Y. D. Yang and X. Zhang, JHEP **1608**, 054 (2016) doi:10.1007/JHEP08(2016)054 [arXiv:1605.09308 [hep-ph]]; N. G. Deshpande and X. G. He, arXiv:1608.04817 [hep-ph]; S. Nandi, S. K. Patra and A. Soni, arXiv:1605.07191 [hep-ph]; S. Sahoo, R. Mohanta and A. K. Giri, arXiv:1609.04367 [hep-ph].

[15] Y. Sakaki, M. Tanaka, A. Tayduganov and R. Watanabe, Phys. Rev. D **88**, no. 9, 094012 (2013) doi:10.1103/PhysRevD.88.094012 [arXiv:1309.0301 [hep-ph]];

[16] P. Biancofiore, P. Colangelo and F. De Fazio, Phys. Rev. D **87**, no. 7, 074010 (2013) doi:10.1103/PhysRevD.87.074010 [arXiv:1302.1042 [hep-ph]]; R. Dutta, A. Bhol and A. K. Giri, Phys. Rev. D **88**, no. 11, 114023 (2013) doi:10.1103/PhysRevD.88.114023 [arXiv:1307.6653 [hep-ph]]; Y. Sakaki, M. Tanaka,

A. Tayduganov and R. Watanabe, Phys. Rev. D **91**, no. 11, 114028 (2015) doi:10.1103/PhysRevD.91.114028 [arXiv:1412.3761 [hep-ph]]; R. Alonso, A. Kobach and J. Martin Camalich, arXiv:1602.07671 [hep-ph]; A. K. Alok, D. Kumar, S. Kumbhakar and S. U. Sankar, arXiv:1606.03164 [hep-ph]; D. Bardhan, P. Byakti and D. Ghosh, arXiv:1610.03038 [hep-ph]; Z. Ligeti, M. Papucci and D. J. Robinson, arXiv:1610.02045 [hep-ph]; N. Kosnik, arXiv:1610.00447 [hep-ph].

[17] I. Caprini, L. Lellouch and M. Neubert, Nucl. Phys. B **530**, 153 (1998) doi:10.1016/S0550-3213(98)00350-2 [hep-ph/9712417].

[18] B. Aubert *et al.* [BaBar Collaboration], Phys. Rev. Lett. **104**, 011802 (2010) doi:10.1103/PhysRevLett.104.011802 [arXiv:0904.4063 [hep-ex]].

[19] W. Dungel *et al.* [Belle Collaboration], Phys. Rev. D **82**, 112007 (2010) doi:10.1103/PhysRevD.82.112007 [arXiv:1010.5620 [hep-ex]].

[20] J. G. Körner and G. A. Schuler, Z. Phys. C **46**, 93 (1990). doi:10.1007/BF02440838

[21] J. A. Bailey *et al.* [MILC Collaboration], Phys. Rev. D **92**, no. 3, 034506 (2015) doi:10.1103/PhysRevD.92.034506 [arXiv:1503.07237 [hep-lat]].

[22] Y. Amhis *et al.* [Heavy Flavor Averaging Group (HFAG) Collaboration], arXiv:1412.7515 [hep-ex].

[23] J. A. Bailey *et al.* [Fermilab Lattice and MILC Collaborations], Phys. Rev. D **89**, no. 11, 114504 (2014) doi:10.1103/PhysRevD.89.114504 [arXiv:1403.0635 [hep-lat]].

[24] Andrae, R., Schulze-Hartung, T., & Melchior, P. 2010, arXiv:1012.3754

[25] `http://cernlib.web.cern.ch/cernlib/`

[26] R. Aaij *et al.* [LHCb Collaboration], Phys. Lett. B **708**, 241 (2012) doi:10.1016/j.physletb.2012.01.058 [arXiv:1112.4896 [hep-ex]].

[27] K. A. Olive *et al.* [Particle Data Group Collaboration], Chin. Phys. C **38**, 090001 (2014). doi:10.1088/1674-1137/38/9/090001

[28] Shibata, Ritei. "An Optimal Selection of Regression Variables." Biometrika 68, no. 1 (1981): 45-54.

[29] Box, G.E.P., and Jenkins, G.M. (1970). *Time series analysis: forecasting and control.* Holden-Day, London.

[30] Breiman L. (1992). The little bootstrap and other methods for dimensionality selection in regression: X-fixed prediction error. *Journal of the American Statistical Association* **87**, 738754.

[31] Akaike, H. (1973). Information theory as an extension of the maximum likelihood principle. Pages 267281 in B. N. Petrov, and F. Csaki, (eds.) *Second International Symposium on Information Theory.* Akademiai Kiado, Budapest.

[32] Sugiura, N. (1978). Further analysis of the data by Akaikes information criterion and the finite corrections. *Communications in Statistics, Theory and Methods* **A7**, 1326.

[33] Akaike, H. (1983). Information measures and model selection. *International Statistical Institute* **44**, 277291.

[34] S. S. Wilks, Annals Math. Statist. **9**, no. 1, 60 (1938). doi:10.1214/aoms/1177732360